# Modeling and simulating the growth of ellipsoidal droplets during dropwise condensation on pillared surfaces

Solmaz Boroomandi Barati, Victor Rabiet, Jean-Charles Pinoli, Yann Gavet, Stéphane Valette

# Modeling and simulating the growth of ellipsoidal droplets during dropwise condensation on pillared surfaces

S. Boroomandi Barati*[1], V. Rabiet[2], J.-C. Pinoli[2], S. Valette[3], and Y. Gavet[2]

[1]Univ Lyon, Ecole Nationale Supérieure des Mines de Saint-Etienne, LGF UMR CNRS 5307, SAINT-ETIENNE, France
solmaz.boroomandi@emse.fr
[2]Ecole Nationale Supérieure des Mines de Saint-Etienne, LGF UMR CNRS 5307, SAINT-ETIENNE, France
[3]Univ Lyon, Ecole Centrale de Lyon, LTDS UMR CNRS 5513, F-69134, LYON, France

**Abstract**

A numerical simulation model is proposed to describe ellipsoidal droplets growth on pillared substrates during dropwise condensation. Comparison between gray scale images taken from droplets growing on pillared surfaces with those growing on flat surfaces shows considerable differences that must be taken into account in the simulation model. Firstly, since the droplets can be easily canalized between the pillars, the shape of droplets change from spherical to ellipsoidal specially in coalescence step. Secondly, on pillared surfaces due to droplets three dimensional configuration, coalescence can occur in all three dimensions. And thirdly, if a droplet touches a pillar, they will stay in touch until the end of the process. The model proposed here calculates the growth rate of ellipsoidal droplets during adsorption and coalescence steps, and checks the coalescence by verifying the existence of real intersection between each pair of droplets. The results of this model is compared with real data from 6 different configurations of pillars. The mean relative error of the model for droplets density is $10.00 \pm 0.68\%$, while it proposes more accurate results for predicting droplets radius with the mean error of $2.28 \pm 0.42\%$.

*Keywords*: Dropwise condensation, textured surface, ellipsoidal droplets, numerical simulation

## 1 Introduction

Condensation occurs when the temperature of a mixture of humid air or a pure vapor goes below of its dew point [1]. This process can happen homogeneously, when the small droplets form directly from the humid air (or pure vapor) or heterogeneously, when there is a cold substrate on which the droplets can nucleate.

This process can play a great role in improving the energy utilization and relieving pollution problems [2] and is widely used in heat transfer devices, power generation refrigeration, and waste heat recovery condensers [3, 4]. The efficiency of these devices depends on the mode of condensation, because it has been proved that dropwise mode of condensation has considerably

*corresponding author

greater heat transfer coefficient with respect to filmwise condensation [5]. On the other hand, when condensation occurs as an undesirable process, like what happens on a humid day inside the car light shields, the filmwise mode is more favored. So, there is always a challenge between choosing dropwise or filmwise condensation depending on the application of the system. Beysens did considerable researches on the formation, determination and growth of dew under different situations [1, 6, 7, 8]. Up to now the process of dropwise condensation was mostly studied on flat surfaces [9, 10] or surfaces with coatings [11, 12] since by improving surface hydrophobicity, the mode of condensation will be changed considerably. The more hydrophobic the surface, the higher percentage of dropwise condensation with respect to filmwise will occur. Vemuri and Kim [11] reported the increase of about 8 times in condensation heat transfer rate on the hydrophobic coating of *n*-octadecyl mercaptan with respect to complete filmwise condensation under atmospheric pressure. Tiang *et al.* [12] compared the rate of droplets growth on two hydrophobic surfaces, a polymer film and a silanized glass slide. Xiuliang and Cheng [13] studied the effect of coating thickness, thermal conductivity of coating and contact angle on the heat transfer during dropwise condensation. They also improved a thermodynamic model to calculate the critical radius for dropwise condensation on sub-cooled coated surface [14]. The problem with chemical coatings is their harmful effects on environment and waste water. These drawbacks provoked the interests for studying other methods to achieve dropwise condensation in last few years.

On the other hand, changing surface roughness and surface morphology can also control the proportion of dropwise and filmwise condensation [15]. Water droplets on pillared hydrophobic surfaces generally exhibit two morphologies: the Wenzel state [16] and the Cassie state [17]. Cassie droplets are in contact with peaks of the pillars, under which the "air pockets" are trapped (figure 1-a), while Wenzel droplets are in full contact with the surface and are able to wet it (figure 1-b) [18]. Chen *et al.* [19] discovered that Cassie droplets are more stable than Wenzel type on the rough surfaces with micro and nano-pillars. Qian and Ma [20] stated that nano-concave or convex topography can change nucleation pattern of droplets on a rough surface.

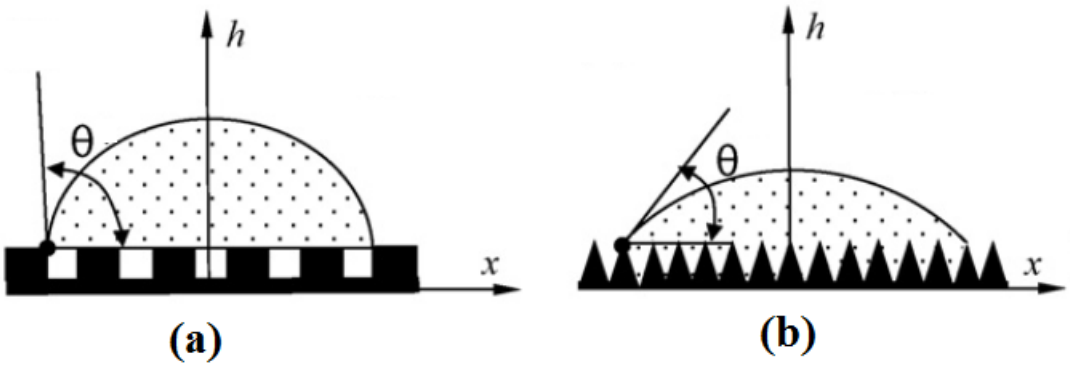


Figure 1: (a) Cassie-baxter and (b) Wenzel droplets on textured surfaces (image from [21]).

The effect of surface topography on the droplets nucleation was investigated by a lot of authors [20, 22, 23, 6]. Recently S.Zarei *et al.* [24] studied the effect of different topographies on the growth rate of water droplets. They considered two texturing patterns semi-conical and semi-pyramidal geometries and their limit states, prismatic and cylindrical geometries. They also considered the effect of the size of texturing patterns as well as the roughness parameters on the temperature drop and total heat transfer.

But there is a lack of studies dealing with presenting a model describing droplets growth on the textured surfaces. This is because of the complexity of the droplets shape on textured surfaces. Generally on micro-textured surfaces droplets are more ellipsoidal than spherical, because they

tend to make a canal of liquid between the texturations. This difference can be seen in figure 2. Figure 2-A shows the spherical droplets growing on a flat surface, while figure 2-B shows the ellipsoidal droplets on a micro-pillared substrate. On the other hand, the position of droplets on textures substrates can be influenced by the pattern of the surface and is not as easily predictable as on the flat substrate.

It must be taken into account that the shape of droplets depends on their size and the size of texturing patterns. That is why usually nano-texturing patterns do not change the shape of droplets.

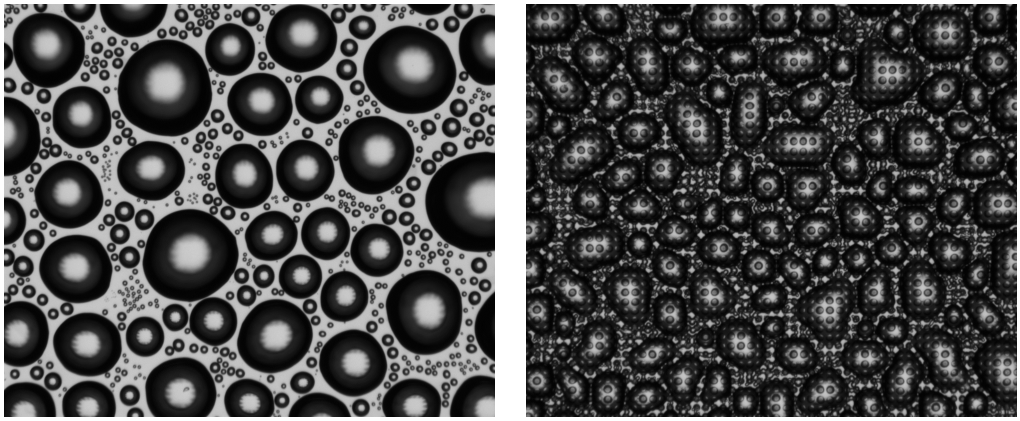

(A) (B)

Figure 2: Differences between shape of droplets on the flat and pillared surfaces, (A) spherical droplets growing on a flat surface, (B) ellipsoidal droplets growing on a pillared surface. The small circles in image (B) are the pillars. Images are obtained from the home-made experimental set-up. The size of the substrate at each image is $3.3mm \times 2.7mm$.

The aim of this research is to present a novel method to simulate ellipsoidal droplets growth on different pillared surfaces. The results of this algorithm are validated by comparison with experimental data on six different patterns of the pillared surfaces. The experiments are carried out on the poly carbonate surfaces that are duplicated from a metal mold textured using laser technology, without any chemical and harmful coatings.

## 2 Growth rate of ellipsoidal droplets

As it was explained in our former works [25, 26], the process of dropwise condensation consists of four main steps: nucleation of initial droplets, growth rate due to adsorption, growth rate due to coalescence followed by nucleation of new small droplets, and sliding of the very big droplets from the surface. There are two kinds of growth procedures for each droplet regardless of its size and shape:

- Growth rate due to adsorbing water molecules from humid air.
- Growth rate due to coalescence, that refers to the process of merging two or more touching droplets to form a bigger one called daughter droplet.

For a spherical droplet, the sizes in all the directions are the same and equal to $r$. This kind of droplets with related equation can be seen in figure 3-A. Figure 3-B shows an ellipsoidal droplet with its major diameters $a$, $b$, and $c$ in the directions of $X$, $Y$, and $Z$, respectively. We will consider $b = e.a$ and $c = f.a$, where $e$ and $f$ are the ratios between $Y$-direction and $Z$-direction radius of ellipsoid with respect to its $X$-direction radius. We consider that droplets form on $X$-$Y$ plane and $Z$ is the direction of their height.

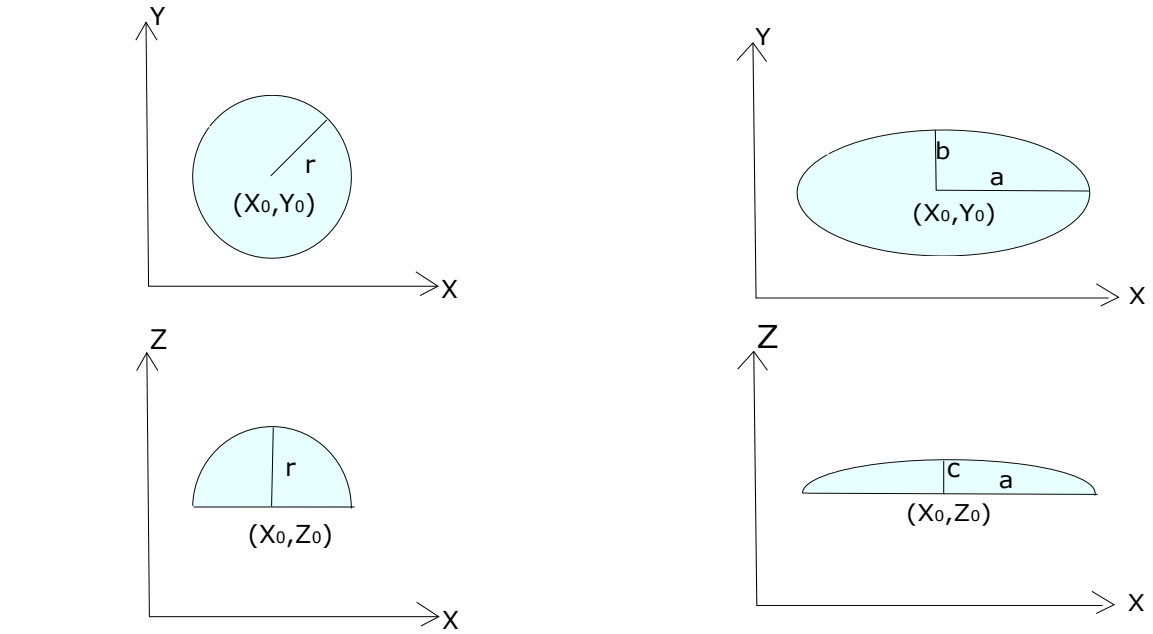


$\frac{1}{r^2}(X-X_0)^2+\frac{1}{r^2}(Y-Y_0)^2+\frac{1}{r^2}(Z-Z_0)^2=1$ (A)

$\frac{1}{a^2}(X-X_0)^2+\frac{1}{b^2}(Y-Y_0)^2+\frac{1}{c^2}(Z-Z_0)^2=1$ (B)

Figure 3: Schematic of (A) hemi-spherical droplets and (B) hemi-ellipsoidal droplets in two planes ($X$-$Y$) and ($X$-$Z$) and their corresponding equations. Droplets form on $X$-$Y$ plane and $Z$ is the direction of their heights.

### 2.1 Adsorption

The growth rate due to adsorption for hemi-spherical droplets on flat substrates can be calculated by equaling the latent heat of condensation:

$$q=\rho_l H_{fg}\pi r^2(1-Cos\theta)^2(2+Cos\theta)\frac{dr}{dt}, \tag{1}$$

and the heat flux through a droplet:

$$q=\frac{\Delta T_{sat-wall}-\frac{2T_{sat}\sigma}{H_{fg}\rho r}}{\frac{1}{2\pi r^2 h_i(1-Cos\theta_a)}+\frac{\theta_a}{4K_w\pi r Sin\theta_a}}. \tag{2}$$

Here $\Delta T_{sw}$ indicates the difference between substrate temperature and air saturated temperature, $\rho$ is water density, $H_{fg}$ water latent heat, $h_i$ interfacial condensation heat transfer coefficient, $\theta$ mean contact angle, and $K_w$ is water thermal conductivity. $h_i$ can be calculated as follow:

$$h_i=\frac{2\alpha}{2-\alpha}\sqrt{M/2\pi\dot{R}T_{dew}}\frac{H_{fg}^2}{T_{dew}v_g}, \tag{3}$$

where $v_g$ is specific volume of gas phase, $M$ is molecular weight of water and $\dot{R}$ is the gas universal constant. $\alpha$ is the condensation coefficient related to non-condensable gases mixed with air. For pure vapor $\alpha=1$, while in the case of humid air or the presents of any other non-condensable gases $\alpha<1$.

In equation (2) two heat transfer resistances between air and temperature have been considered: conduction $R_h=\frac{1}{2\pi r^2 h_i(1-Cos\theta_a)}$ and convection $R_c=\frac{\theta_a}{4K_w\pi r Sin\theta_a}$. These resistances are shown in figure 4-A. Also the term $\frac{2T_{sat}\sigma}{H_{fg}\rho r}$ indicates the temperature drop due to droplets curvature. By equaling the two equations (1) and (2), we will have:

$$r_k = r_{k-1} + \Delta t \frac{\mathrm{d}r}{\mathrm{d}t}, \quad \text{and} \quad \frac{\mathrm{d}r}{\mathrm{d}t} = \frac{C_1(1 - \frac{r_{min}}{r})}{C_2 + C_3 r}, \tag{4}$$

where $k$ represents each generation of droplets, $\Delta t$ is the time step, and $C_1 = \frac{1}{(1-\mathrm{Cos}\theta)^2(2+\mathrm{Cos}\theta)} \frac{\Delta T_{sw}}{\rho H_{fg}}$, $C_2 = \frac{1}{2h_i(1-\mathrm{Cos}\theta)}$, and $C_3 = \frac{\theta}{4K_w \mathrm{Sin}\theta}$ [25, 27].

Miljkovic *et al.* [4, 28, 29] have done considerable efforts to calculate the growth rate of jumping and non-jumping cassie-baxter and Wenzel droplets on the super-hydrophobic pillared substrates. In the case of textured substrate, two other resistances will be added to the equation (2): convection throughout the cylindrical pillars $R_p = \frac{H_p}{\varphi \pi r^2 k_p \sin^2\theta}$, and convection throughout the liquid band between the pillars $R_l = \frac{H_p}{(1-\varphi)\pi r^2 k_w \sin^2\theta}$. $H_p$, $k_p$, and $\varphi$ are being the pillar height, pillar convection coefficient and the structured surface solid fraction. [24, 15]

These resistances are shown in figure 4-B and C. Considering the summation of the two parallel resistances $R_l$ and $R_p$ as $\Sigma R = \frac{R_l R_p}{R_l + R_p}$, equation (2) will change to:

$$q = \frac{\Delta T_{sat-wall} - \frac{2T_{sat}\sigma}{H_{fg}\rho r}}{\frac{1}{2\pi r^2 h_i(1-Cos\theta_a)} + \frac{\theta_a}{4K_w \pi r Sin\theta_a} + \frac{H_p}{\pi r^2 \sin^2\theta (k_w(1-\varphi)+k_p\varphi))}}. \tag{5}$$

Equaling equations (1) and (5), the growth rate of the droplets on pillared substrates will be calculated as in equation (4), but with different coefficients: $C_1 = \frac{1}{(1-\mathrm{Cos}\theta)^2(2+\mathrm{Cos}\theta)} \frac{\Delta T_{sw}}{\rho H_{fg}}$, $C_2 = \frac{1}{2h_i(1-\mathrm{Cos}\theta)} + \frac{H_p}{\pi r^2 \sin^2\theta (k_w(1-\varphi)+k_p\varphi))}$, and $C_3 = \frac{\theta}{4K_w \mathrm{Sin}\theta}$. These equations show the heat flux and the growth rate of a Wenzel droplet [24], for Cassie droplets since the zone between the pillars is filled by air, we can consider that there is no convection in this area and consider $k_w = 0$ in the last term of the denominator of equation (5) and $C_2$.

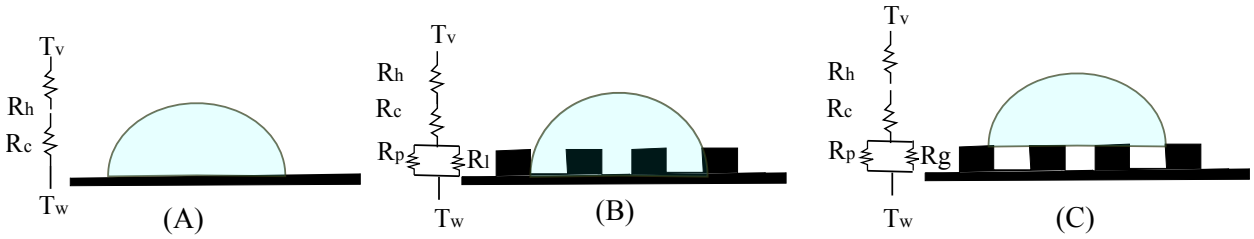


Figure 4: Thermal resistances for heat transfer through (A) a droplet on a flat substrate, (B) a Wenzel droplet on a pillared substrate and (C) a Cassie droplet on a pillared substrate.

If we consider $r$ as the equivalent radius of the ellipse that is the radius of the sphere having the same volume as the ellipse, we will have:

$$r^3 = a.b.c. \tag{6}$$

Considering $b = e.a$ and $c = f.a$ and derivation with respect to $t$ will result in:

$$3r^2 \frac{\mathrm{d}r}{\mathrm{d}t} = (\frac{3e}{f^2}) c^2 \frac{\mathrm{d}c}{\mathrm{d}t}, \tag{7}$$

and thus,

$$\frac{\mathrm{d}c}{\mathrm{d}t} = (\frac{f^2.r^2}{e.c^2}) \frac{\mathrm{d}r}{\mathrm{d}t}, \tag{8}$$

where $\frac{\mathrm{d}r}{\mathrm{d}t}$ can be calculated using equation (4) and the method of Euler in solving ordinary differential equations. And then since $\frac{\mathrm{d}a}{\mathrm{d}t} = \frac{1}{f}.\frac{\mathrm{d}c}{\mathrm{d}t}$ and $\frac{\mathrm{d}b}{\mathrm{d}t} = \frac{e}{f}.\frac{\mathrm{d}c}{\mathrm{d}t}$, it is possible to calculate the

growth rate of an ellipsoidal droplet due to adsorption in all three dimensions and then:

$$\begin{aligned} a_k &= a_{k-1} + \frac{\mathrm{d}a}{\mathrm{d}t}, \\ b_k &= b_{k-1} + \frac{\mathrm{d}b}{\mathrm{d}t}, \\ c_k &= c_{k-1} + \frac{\mathrm{d}c}{\mathrm{d}t}. \end{aligned} \tag{9}$$

At the end, the new values of $e$ and $f$ will be calculated by $e = \frac{b}{a}$, and $f = \frac{c}{a}$.

## 2.2 Coalescence

### 2.2.1 Checking for coalescence

Ellipsoidal droplets can touch in different ways. According to figure 5-A, if the droplets are spherical, the condition for their coalescence can be studied by measuring the Euclidean distance between their center points. If the Euclidean distance between the center points goes beyond the summation of their radius, they will merge and form the so-called daughter droplet. In contrast, there are many ways for approaching two ellipsoidal droplets. Two ellipsoids can touch in the directions of $a_1 - a_2$, $b_1 - b_2$, $a_1 - b_2$, or even in the directions not corresponding to the parameters $a$ and $b$ . So, the best way for studying the condition of coalescence for two ellipsoids is calculating the surface of their intersection that is shown in figure 5-B.

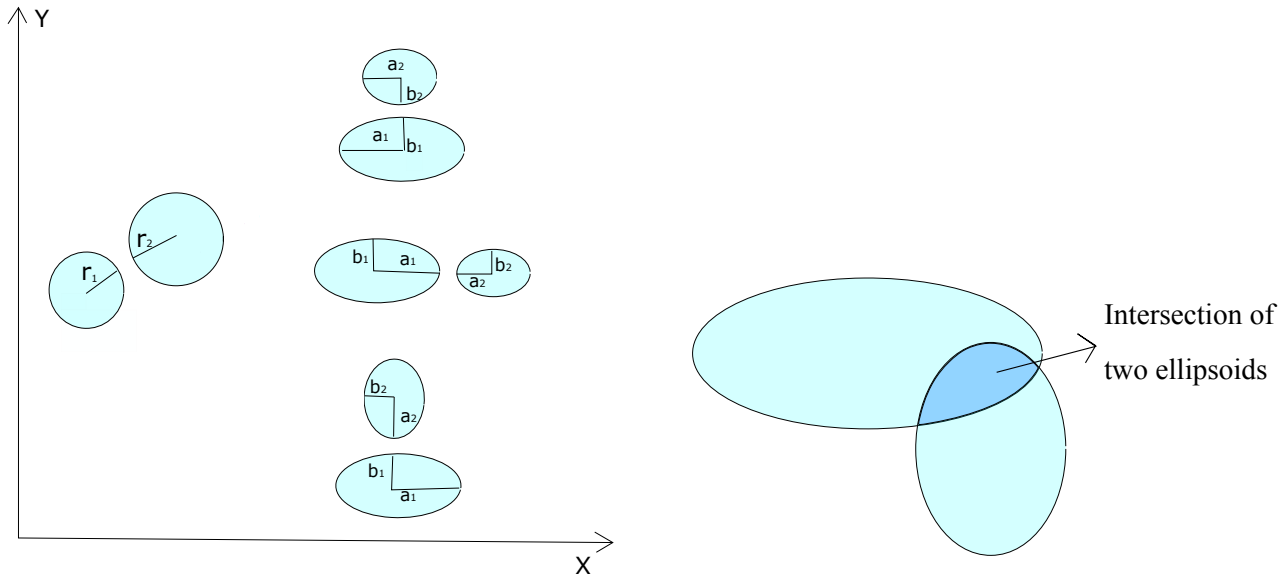


(A) (B)

Figure 5: (A) The difference between approaching two spherical droplets *v.s* two ellipsoidal droplets, (B) intersection of two touching ellipsoidal droplets.

For calculating the intersection between two ellipses in two dimensions, one has to solve the system of equations of two ellipses, considering the point of (0,0) as the center of the first ellipse. So, the equation of the first ellipse will reduce to equation (10), while the second ellipsoid is as indicated in equation (11).

$$\begin{cases} A_1 X^2 + Y^2 = R_1, & (10) \\ A_2 (X - X_0)^2 + (Y - Y_0)^2 = R_2, & (11) \end{cases}$$

where $A_1 = \frac{b_1^2}{a_1^2}$ and $R_1 = b_1^2$, $A_2 = \frac{b_2^2}{a_2^2}$, and $R_2 = b_2^2$. Subtracting equation (11) from equation (10) gives:

$$A_2(X - X_0)^2 - A_1X^2 + (Y - Y_0)^2 - Y^2 = R_2 - R_1, \tag{12}$$

$$Y^2 = A_3^2X^4 + B_3X^2 + C_3^2 + 2A_3B_3X^3 + 2A_3C_3X^2 + 2B_3C_3X, \tag{13}$$

where $A_3 = \frac{A_2 - A_1}{2Y_0}$ , $B_3 = \frac{-2A_2X_0}{2Y_0}$ , $C_3 = \frac{R_1 - R_2 + A_2X_0^2 + Y_0^2}{2Y_0^2}$.

Substituting equation (13) in equation (10), will result in:

$$A_4X^4 + B_4X^3 + C_4X^2 + D_4 + E_4 = 0, \tag{14}$$

where $A_4 = A_3^2$ , $B_4 = 2A_3B_3$ , $C_4 = A_1 + B_3^2 + 2A_3C_3$ , $D_4 = 2B_3C_3$, $E_4 = C_3^2 - R_1$.

Equation (14) represents the equation of the intersection between two ellipses. Two ellipses have intersection if and only if equation (14) has at least one real root, meaning that two droplets touch and coalescence will occur. As was mentioned before, on textured surfaces the droplets are spatially distributed on three dimensional space, consequently coalescence can occur in all three dimensions, but solving the system of equations (11) and (12) for the intersection of 3-dimensional ellipsoids is very complicated. Therefore, for checking coalescence in the 3-dimensional space, we can solve the same system of equation, but in three planes ($X - Y$, $X - Z$, and $Z - Y$).

### 2.2.2 Gowth rate due to coalescence

After the criterion for coalescence is satisfied, the next step is to calculate the size and position of the daughter droplet. The growth rate due to coalescence can be calculated based on the assumption that coalescence is a mass conservative process, meaning that during this process the total amount of liquid will not change. So, for hemi-spherical droplets we can write:

$$V = V_i + V_j \rightarrow r = \sqrt[3]{r_i^3 + r_j^3}, \tag{15}$$

where $V$ and $r$ indicate the volume and radius of daughter droplet resulting from coalescence of droplets $i$ and $j$. If we consider the total volume of liquid present in the coalescence of two hemi-ellipsoidal droplets $i$ and $j$ as:

$$V = (\frac{2\pi}{3})(a.b.c) = (\frac{2\pi}{3})(a_i.b_i.c_i + a_j.b_j.c_j). \tag{16}$$

So, we will have 1 equations and 3 unknown parameters ($a$, $b$, and $c$). For solving this system of equations we will need two assumptions. Therefore, by analogy with equation (15) for hemi-spherical droplets, we will assume $a$ and $b$ of daughter drop as:

$$a = \sqrt[3]{a_i^3 + a_j^3}, \tag{17}$$

$$b = \sqrt[3]{b_i^3 + b_j^3}. \tag{18}$$

These assumptions mean that we consider the small and grand axis of the ellipsoid grow like the radius of a hemi-sphere. Then $c$ can be calculated from equation (16) and finally new $e$ and $f$ will be $e = \frac{b}{a}$, and $f = \frac{c}{a}$.

### 2.2.3 Position of daughter droplet

In the process of coalescence for hemi-spherical droplets, the center point of the daughter drop is at the mass center of its parents named drops $i$ and $j$:

$$\begin{aligned} x &= \frac{r_i^3.x_i + r_j^3.x_j}{r_i^3 + r_j^3}, \\ y &= \frac{r_i^3.y_i + r_j^3.y_j}{r_i^3 + r_j^3}, \\ z &= \frac{r_i^3.z_i + r_j^3.z_j}{r_i^3 + r_j^3}, \end{aligned} \tag{19}$$

where $x$, $y$, and $z$ represent the location of droplets center points. For ellipsoidal droplets the mass center of droplets that is equal to the center point of daughter droplets after coalescence is:

$$\begin{aligned} x &= \frac{(a_i.b_i.c_i).x_i + (a_j.b_j.c_j).x_j}{a_i.b_i.c_i + a_j.b_j.c_j}, \\ y &= \frac{(a_i.b_i.c_i).y_i + (a_j.b_j.c_j).y_j}{a_i.b_i.c_i + a_j.b_j.c_j}, \\ z &= \frac{(a_i.b_i.c_i).z_i + (a_j.b_j.c_j).z_j}{a_i.b_i.c_i + a_j.b_j.c_j}. \end{aligned} \tag{20}$$

The study on real images from pillared surfaces shows that if a droplet touches a pillar, they will stay in touch till the end of process. This fact will add another condition to the coalescence process that is:
If one of the parents is in touch with a pillar, the center point of the daughter drop will not be in mass center of the parents anymore.
So, there will be two situations after coalescence for center of daughter droplets:

- If both of the parents or none of them already touch the pillars, then the center point of daughter will be the same as in equations (20).
- If just one of the parents already touches at least one pillar, then the center point of daughter will be at the center of the parent that is in contact with the pillars.

The first case describes the situation where the adhesive force is linearly proportional to droplet volume like on the flat substrate. One assumption is made here: if both parents touch a pillar, the adhesive forces with the pillars on both of them are the same. But if just one of the parents touches at least one pillar, the adhesive force will make the center point of the daughter at the center point of the parent that is in touch with the pillar.

## 3 Departure of big droplets

For droplets growing on vertical substrates the effect of gravity on the advancement of the process of dropwise condensation must not be neglected. The gravity force will cause the big and heavy droplets to slide and clean off the other droplets on their path. This will introduce more strip area for the nucleation of new small droplets. The adhesive force between a droplet and substrate comes from surface roughness and contact angle hysteresis [30]. The check for departure can be done by comparing the gravity force and adhesive force affecting each droplet. The gravity force for a droplet with advancing and receding contact angles $\theta_a$ and $\theta_r$ is [15, 4]:

$$F_g = \frac{(2 - 3\mathrm{Cos}\theta + \mathrm{Cos}^3\theta)\pi r_{max}^3 \rho_l g}{3}. \tag{21}$$

The adhesive force with the surface can be assumed as the surface tension force [15, 4]:

$$F_\sigma = 2\sigma r_{max} Sin\theta(\text{Cos}\theta_r - \text{Cos}\theta_a). \tag{22}$$

$\theta$ here being the apparent equilibrium contact angle and may be taken equal to $\text{Cos}^{-1}(0.5\text{Cos}\theta_a + 0.5\text{Cos}\theta_r)$ [4]. The shape of droplets also depends on the competition between adhesive force with the texturing and droplets surface tension. In the case of medium droplets, the adhesive force with the pillars makes droplets form more ellipsoidal shape. Whereas, the small and the big droplets that are either too small or huge enough to not be influenced by surface micro texturing, tend to present more spherical shape to occupy less space due to the effect of their surface tension. This effect can be seen in figure 6. On the other hand, since the departing droplets are always huge and heavy droplets, equations (21) and (22) that are developed originally for spherical droplets can be used for verifying droplets departure in this model.

The term small, medium and big here refers to the size of droplets with respect to the size of texturing pattern. From our experiments, for the ratio of droplets to the pillars diameter being at the order of 10-100, the droplets can be considered as medium and will be affected by the texturing pattern and form more ellipsoidal shape. But, the droplets smaller or bigger than this ratio will not be influenced by the texturing pattern and form more spherical shape. It worth pointing out that these values are completely experimental and are announced based on our gray scale figures. S.Zarei *et al.* [24] considered the same definition as Abu-Orabi [31] for small droplets ($r < r_c$) and they stated that the shape of texturing patterns can change small droplets population by about 10%.

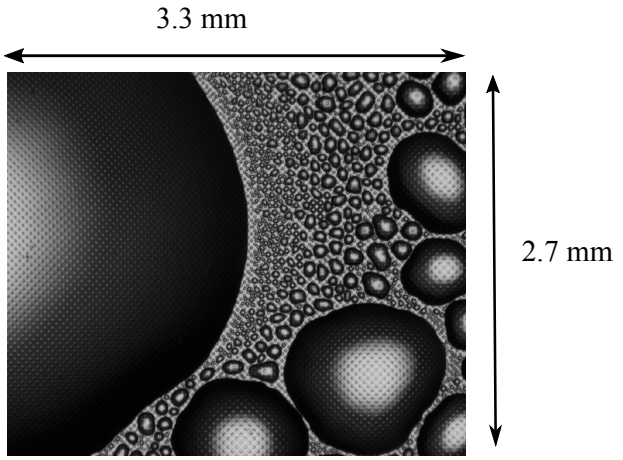


Figure 6: Comparison between the shape of small and big droplets. Small droplets tend to form more ellipsoidal shape due to adhesion with surface texturing, while big droplets present more spherical shape in order to occupy less surface. The size of the substrate is $3.3mm \times 2.7mm$.

## 4 Experimental set-up

Six different metallic molds are textured with uniform patterns of pillars using laser technology. The theoretical radius ($r_p$), theoretical height ($H_p$), and the theoretical distance between the pillars ($D_p$) corresponding to each spatial pattern are presented in table 1. The term theoretical here means that these dimensions are the designed values for pillars and they must be validated by microscopical measurements. In this table, six substrates are named as configuration 1, configuration 2, ..., and configuration 6. These molds then are duplicated by melted poly carbonate, in order to prepare the pillared substrates that are able to be applied during the process of dropwise

Table 1: Surfaces characterization.

| configuration of surface | $r_p(\mu m)$ | $D_p$ $(\mu m)$ | $H_p$ $(\mu m)$ | $R_a(\mu m)$ | $\theta(^\circ)$ | $\theta_a(^\circ)$ | $\theta_r(^\circ)$ |
|---|---|---|---|---|---|---|---|
| configuration 1 | 12.5 | 50 | 3 | 0.31 | 100.2 | 100.0 | 44.1 |
| configuration 2 | 12.5 | 125 | 3 | 0.09 | 97.0 | 99.6 | 54.2 |
| configuration 3 | 25 | 60 | 10 | 0.31 | 102.4 | 101.8 | 41.1 |
| configuration 4 | 25 | 65 | 10 | 0.19 | 105 | 101.8 | 41.1 |
| configuration 5 | 25 | 100 | 10 | 0.17 | 106 | 106.6 | 54.0 |
| configuration 6 | 25 | 150 | 10 | 0.10 | 84.5 | 98.3 | 62.4 |

condensation. The microscopical measurements, then are carried out by a Veeco optical microscope with magnification of 50X in order to validate the size and distance between the pillars. In figures 8 and 9 the illustrations of 6 poly carbonate substrates are presented from macroscopic and microscopic points of view. Roughness value of each substrate ($R_a$) measured by the optical microscope is presented in the fifth column of table 1.

The three last columns of table 1 represent the values of water droplet contact angle on the substrates ($\theta$), as well as advancing and receding contact angles ($\theta_a$ and $\theta_r$). The values of $\theta$ are measured by a DSA30 set-up made by KRUSS. The main part of this set-up is illustrated in figure 7. As shown in this image, the polymeric sample is placed on the substrate support emphasized by (a). The sample is cleaned before, by distilled water and dried by Nitrogen in order to remove any contamination. On the syringe shown in (b) water droplets with volume $3\mu l$ with speed of $100\mu l/min$ are formed at room temperature through a needle with diameter of $500\mu m$. Parts (c) and (d) in this figure show the light source and CCD camera that takes images of droplets sited on the substrate. In order to measuring $\theta_a$ and $\theta_r$, another $7\mu l$ of water is added to the droplets with speed of $10\mu l/min$, and then the adsorbing part is started with the same speed until the droplet is adsorbed completely.

This process is repeated on three substrates of each pillared pattern and the average of $\theta$, $\theta_a$ and $\theta_r$ are presented in table 1.

These six textured surfaces are then used as substrate to grow water droplets during a process of dropwise condensation. Experimental set-up is completely explained in our former article [32]. Generally, each surface is inserted inside a humid chamber with relative humidity of about 40% and air temperature of 303 K. The textured substrate temperature is fixed at 281 K that is one degree below the air mixture dew point. A CCD gray-scale camera records the optical images of droplets that are growing on the textured surface at each second for near $3000s$. This camera uses a long-focal-distance adjustable lens in order to record the high spatial resolution of $1.34 \pm 0.04\mu m/pixel$. These gray scale images are binarized with the image processing method that is presented in our earlier work [33]. The binarized images then are used to extract the information related to the size and droplets density in order to validate the results of the presented method.

## 5 Algorithm for simulating droplets nucleation and growth

The algorithm for simulating nucleation and growth of droplets on pillared surfaces is presented in figure 10. The first step is to simulate the pillars as cylinders with the specified geometric patterns that are presented in table 1. Then, the random ellipses with the same densities as the real droplets (extracted from the binarized images from experimental set-up) are distributed on the 3-dimensional pillared substrate. For the six pillars configuration mentioned here, the droplets initial density is between $10^{12}$ and $10^{13}m^{-2}$ with the equivalent radius around $5 \pm 0.2\mu m$.

These values come from the gray scale images taken from the real droplets growing on the six pillared substrates during the experimental procedure explained in section 4. The initial nucleation densities ($N_D$) for each substrate is presented in table 2.

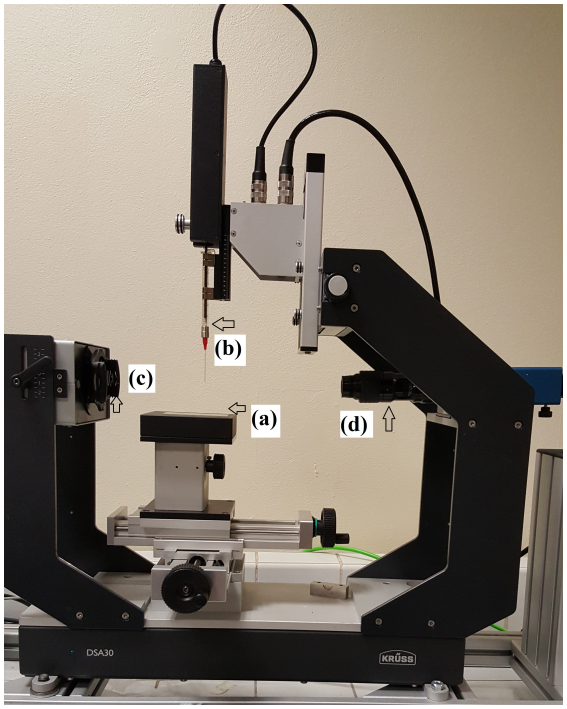


Figure 7: Illustration of contact angle measurement set-up. (a) the substrate support, (b) the syringe for injection water droplets on the substrate, (c) light source, and (d) the CCD camera that acquires images of droplets sited on the substrate.

Table 2: Initial nucleation densities for each substrate.

| configuration of surface | $N_D(m^{-2})$ |
|---|---|
| configuration 1 | $3 \times 10^{13}$ |
| configuration 2 | $4.2 \times 10^{12}$ |
| configuration 3 | $1.9 \times 10^{13}$ |
| configuration 4 | $5.4 \times 10^{13}$ |
| configuration 5 | $6.3 \times 10^{12}$ |
| configuration 6 | $4.2 \times 10^{13}$ |

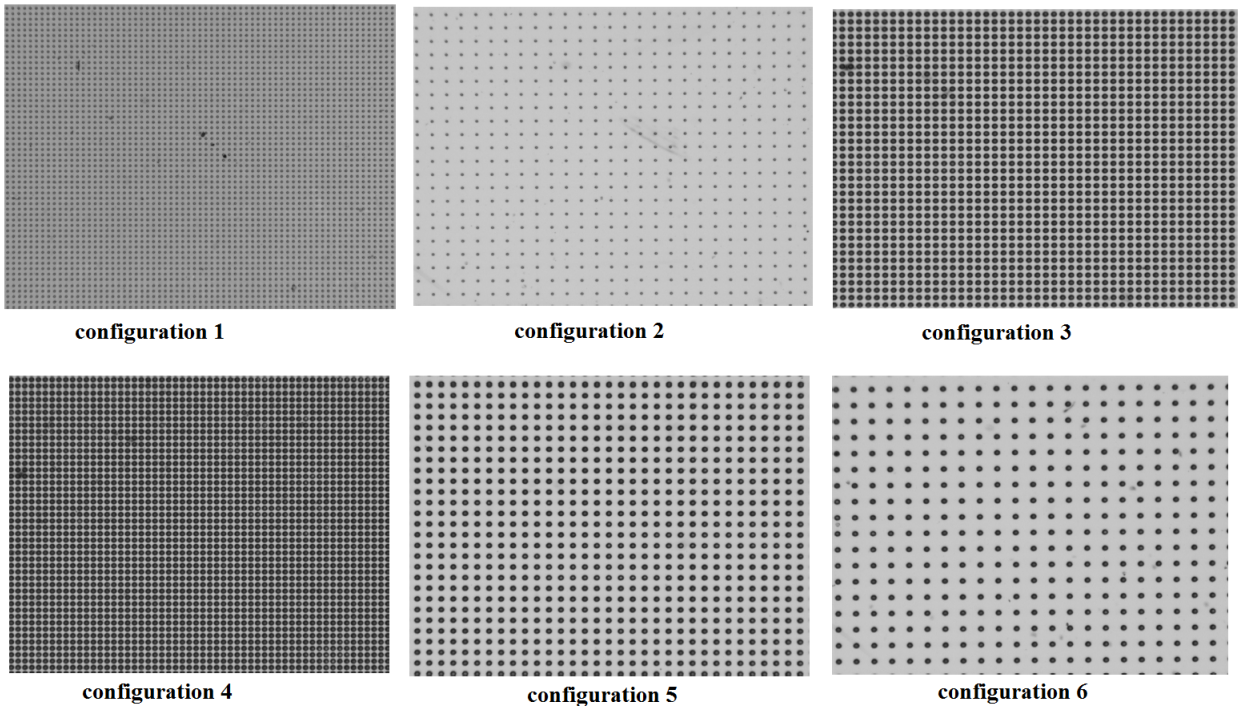


Figure 8: Illustration of six poly carbonate pillared surfaces. The size of the substrate at each image is $3.3mm \times 2.7mm$. The black circles represent the pillars with dimensions according to table1.

Since on a textured surface the droplets can locate at different positions with respect to texturing, there will be a 3-dimensional configuration of droplets that can approach in the directions of $X$, $Y$, or $Z$. On a uniform pillared surface the height of each droplet can be calculated by measuring the spatial distance between its center point and the pillars in its vicinity ($D$):

- if $D > r_p$ : droplet nucleates on the substrate, $z = 0$,
- if $D < r_p$ : droplet nucleates on the top of the pillar, $z = H_p$,
- if $D = r_p$ : droplet nucleates on the side of the pillar, $0 < z < H_p$,

$r_p$ here is the radius of the pillar. The dimensions of each ellipse are considered as $a$ (radius along axis $X$), $b = e.a$ (radius along axis $Y$) and $c = f.a$ (radius along axis $Z$), where $e$ and $f$ are random numbers. The small ellipses also nucleate in the vacant area of substrate at each iteration.

Since the base of this simulation algorithm is to generate the initial droplets of each generation uniformly, we chose six random numbers based on the Poisson point process to describe these droplets: $X$, $Y$, and $Z$ that are the parameters related to the droplets location and $a$, $b$, $c$ that describe droplets size. Based on the experimental data $a$, $b$, and $c$ are generated at the interval of $6.5 \times 10^{-6} \pm 10^{-7}$, then $f = b/a$, $e = c/a$.

Then, all these ellipses grow by adsorbing water molecules from humid air according to the process explained at section 2.1. At each iteration there is a check for recognition the droplets sticking to at least one pillar. This is because, as was mentioned in section 2.2.3, if one of the parent droplets is in contact with a pillar, then the location of the daughter droplet after coalescence will be at its center point. In the next step, the ellipsoidal droplets that are in touch at each of the planes $X - Y$, $X - Z$, or $Y - Z$ are detected by verification the existence of the real root of their intersection equation according to the method proposed in section 2.2.1. These droplets will merge and the size and center point of their daughter droplet is calculated according

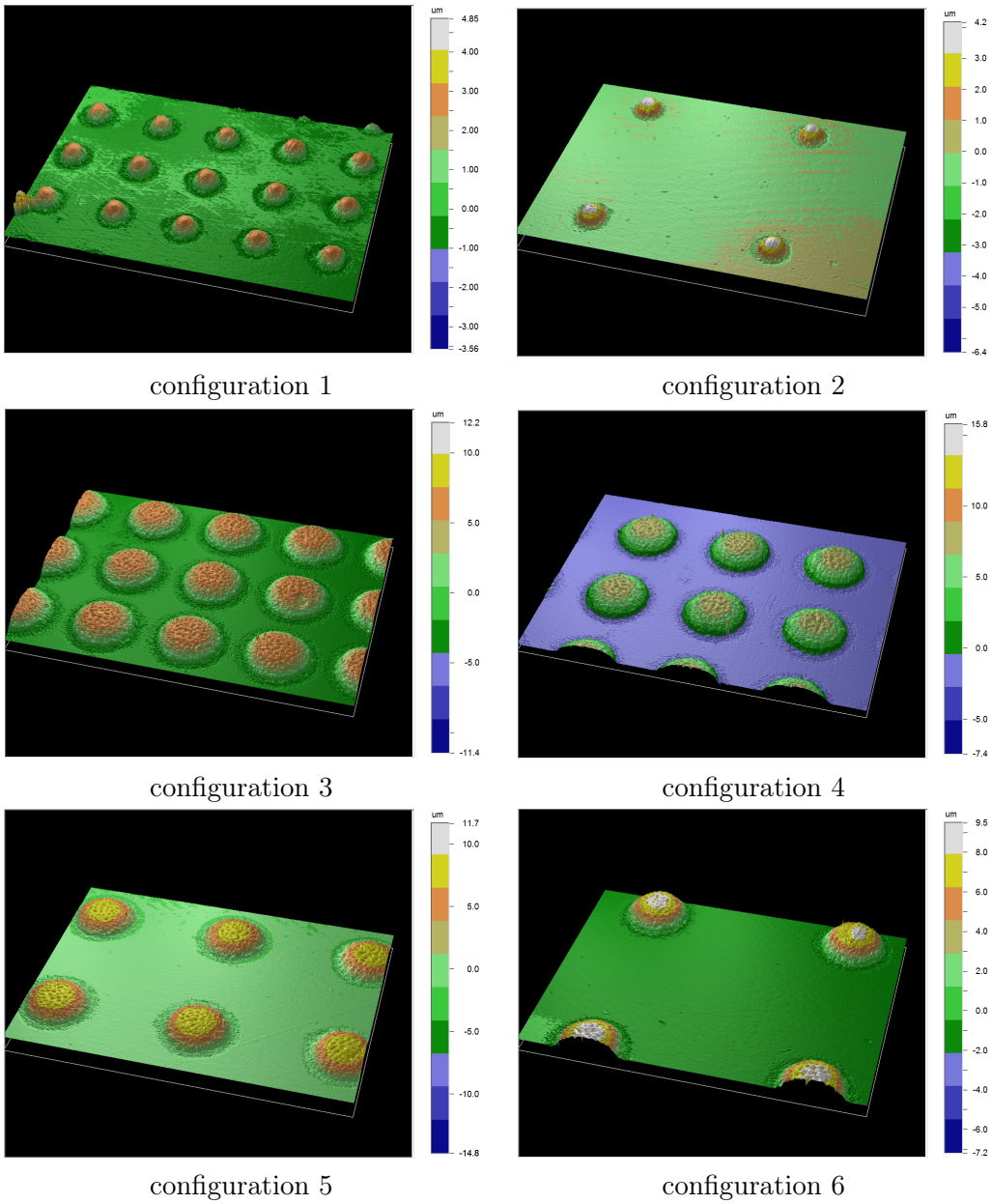


Figure 9: 3-dimensional microscopic illustration of 6 pillared substrates with 50X magnification. The colored bar on the right hand side of each image measures the height of the pillars. Meaning that each color on this bar corresponds to a value on $\mu m$, so for measuring the height of each pillar it is enough to find the value corresponds with the color of it's top head.

to sections 2.2.2 and 2.2.3 respectively. As was explained in section 3, if a droplet becomes big enough to overcome the surface tension, it will slide and clean off all the droplets on its path and will expose strip area to nucleate new small droplets. At the end, the difference between the mean radius of droplets with the mean radius of the droplets in the former iteration is calculated and if it is negligible (less than $10^{-7}m$) the program will stop iterating. The choice of time interval is very important here, because the smaller time steps give more accurate answers but need a huge calculation time. This algorithm works with a time interval of $10^{-4}s$ for solving the Euler method for the growth rate due to adsorption, but the data are compared with experimental values at each $10s$ to be able to illustrate wider time ranges in the graphs. The program was written in matlab and was run on a pair cores PC with Intel Xeon CPU E5-2630 (2.40GHz), with 20gb RAM and it took around 1 hour till completing in around 220 steps. It is worth to point out here that the new method for checking the coalescence that is presented in section 2.2.1 needs considerably less computation time with respect to traditional methods based on measuring the Euclidean distance between the droplets.

# 6 Results and discussion

Figures 11 and 12 show the 2-D roughness profile of the six substrates measured by Veeco optical microscope with magnification of 50X. At each graph, the two cursors measure the distance between a pair of specific points in the directions of $X$ and $Z$ on the substrate. In figure 11, $X$ measures the distance between two pillars centers. This value is shown in table 1 by $D_p$. Figure 12 is a closer point of view to measure the radius and height of pillars on each substrate. $X$ and $Z$ can be compared with the values of $r_p$ and $H_p$ in table 1 respectively.

According to these images there is acceptable accordance between sizes and distances of the pillars and the theoretical data presented in table 1, but the pillars are not perfectly cylindrical as was assumed in the simulation algorithm. It can be clearly seen that the top heads of pillars in all configurations are rounded and dome shaped. Another assumption that is made in the simulation algorithm is that the spatial distribution of droplets on the surface is randomly. This is because the dimension of pillars are fairly bigger than the size of initial generation and one can assume that there is no preference between different spots on the substrate for nucleation of initial small droplets.

Figures 13 and 14 Illustrate the four stages of the droplets growth on surface configuration 5. Figure 13 represents the real droplets growing under the conditions explained at section 4, while figure 14 illustrates the growth procedure of the droplets generated through the simulating algorithm. In both of the figures the first image shows the pillars just before droplets nucleation. According to these figures, at the first stages that the droplets grow mainly by adsorption, the droplets are more circular. After a while that the main growth rate is due to coalescence, the shape of droplets changes to ellipsoidal, but the bigger droplets that are big enough to not be influenced by the texturing pattern become circular again.

The gray scale images of all six substrates at $t = 1800s$ are presented in figure 15. Comparison between these images and data from table 1 reveals that when the pillars are smaller, the final droplets are bigger and their shape is fairly far from being circular. This is because on the surfaces with smaller pillars, the droplets that are growing on the top of a specified pillar, reach the size of the pillar at earlier stages. So, they can slide from the pillar sooner and can join the other droplets that were positioned on the other pillars. Consequently, the droplets can cover several pillars sooner and form a huge area covered by liquid. While, when pillars are bigger, it takes quite long time for droplets to become big enough to slide from the pillar and join with other droplets. By comparing the water droplets on surfaces of configurations 1 and 2 with the surfaces of configurations 3 and 4, one can conclude that when more percentage of substrate is occupied by pillars, the resulting droplets are smaller and consequently more circular. Also, in substrates with configurations 3, 4, 5, and 6 that the height of pillars are $10\mu m$, the droplets are less spread and are mostly connected between two pillars, while in the first 2 surfaces that the height of

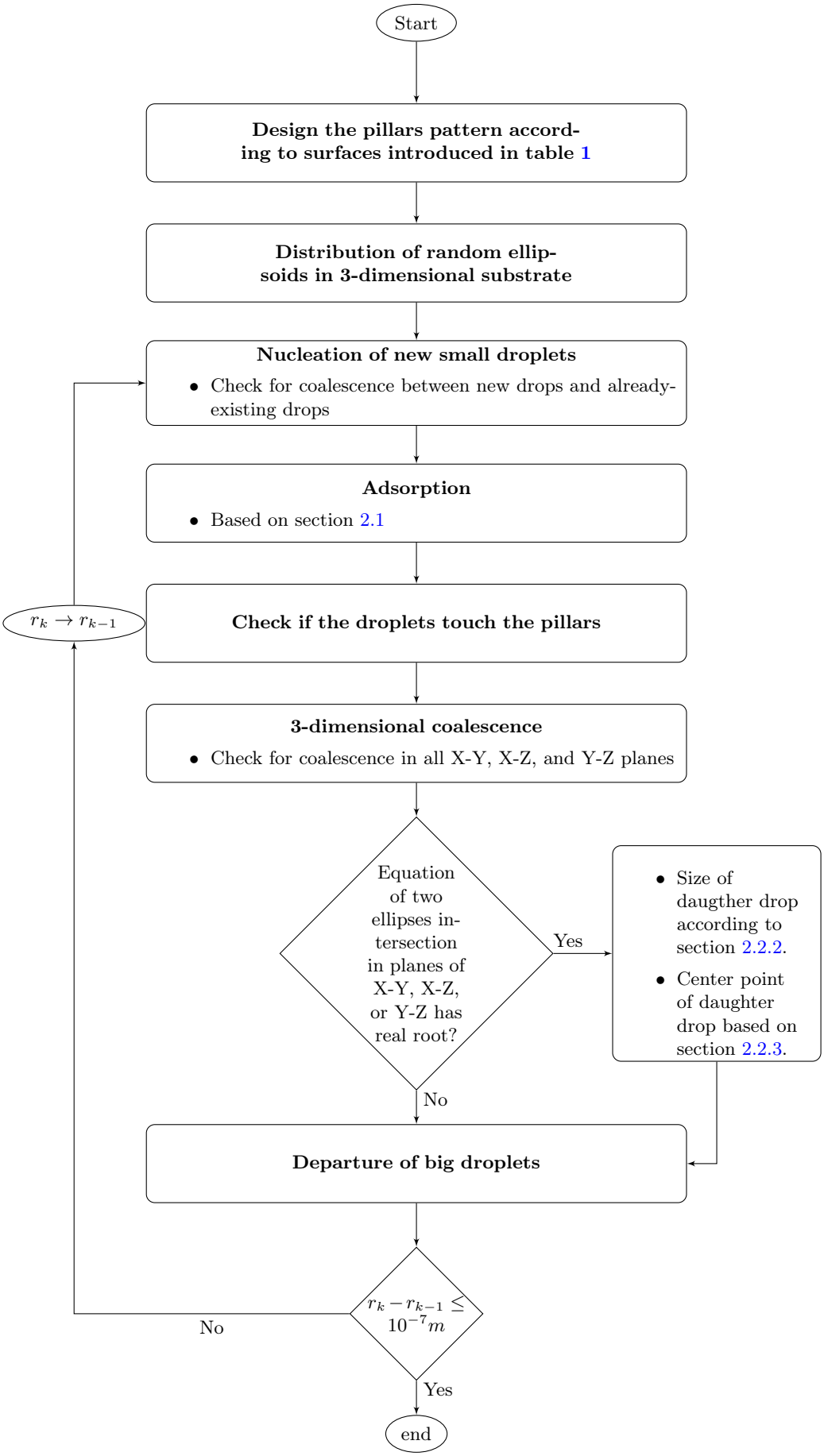


Figure 10: Schematic diagram of the simulation algorithm.

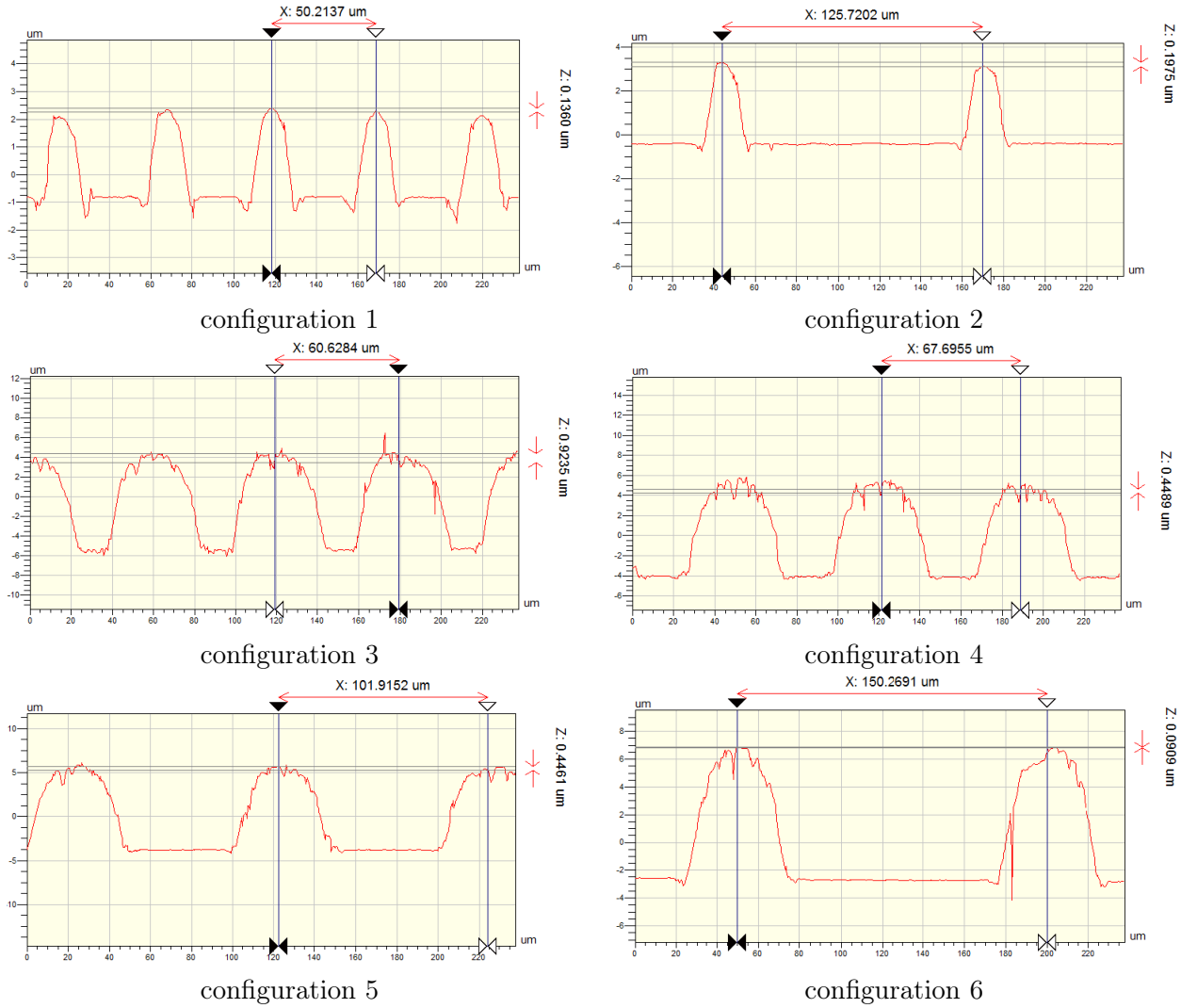


Figure 11: Illustration of 2-D roughness profile of the six substrates. At each graph, $X$ is the distance between the pillars.

pillars is $3\mu m$ the droplets lie on the area of several droplets.

Figures 16 and 17 show the comparison between growth rate and changes in droplets density predicted by the proposed model and real droplets on the six different configurations of pillars.

In these graphs the blue solid lines represent the experimental results that are extracted from the gray scale images of the experimental set-up under the conditions named at section 4 (relative humidity of about 40%, air temperature of 303 K, and substrate temperature of 281 K). The black dashed lines corresponds to the simulation results under the same operating conditions.

It must be pointed out here that in all of the surfaces studied here the critical radius is around $10^{-7}m$. Meaning that the droplets smaller than this value grow by adsorption, while for the droplets bigger than this size the growth rate is mainly due to coalescence. But the rate of coalescence for bigger droplets (between almost 500-1000 $s$) is much bigger than for the smaller droplets (before $500s$).

All these graphs show that the ellipsoidal-droplet model can predict real droplets behavior on the pillared surface very well. At first, in all the surfaces very small droplets start to nucleate between and on the top of the pillars. Since the radius of the pillars are fairly bigger than the radius of the initial droplets, we can assume that there is not considerably preference on top of the pillars for growing very small droplets. According to these graphs, surface with configuration 2 that introduces more flat area, is more potential to nucleate initial droplets. The same pattern

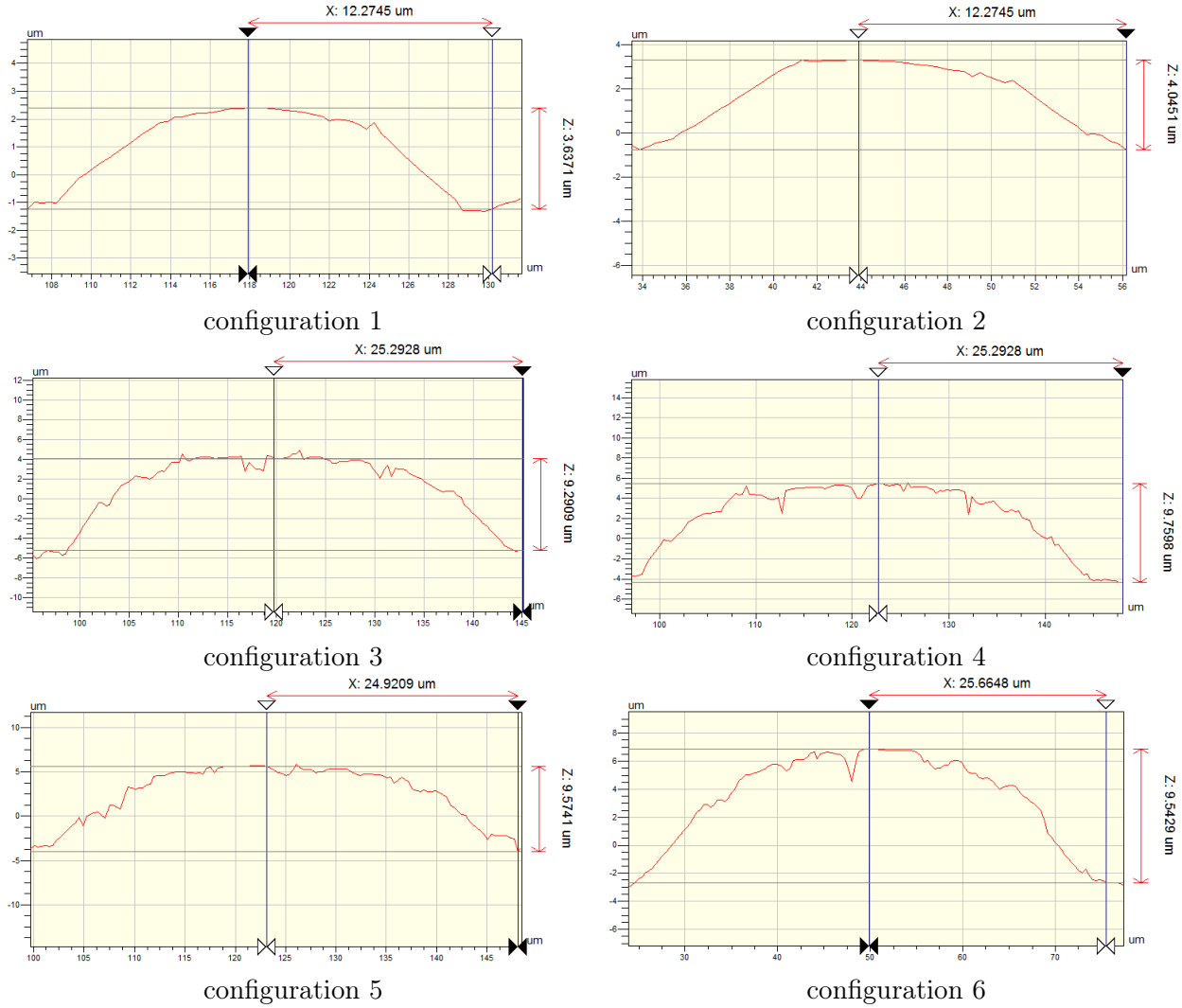


Figure 12: Illustration of 2-D roughness profile of the six substrates. At each graph, $X$ and $Z$ represent the radius and height of the pillars respectively.

in all the surfaces can be considered after this step: all the droplets grow by adsorbing water molecules, if they touch they will coalesce and form bigger droplets and introduce more bare area to nucleate new small droplets. As was expected, the first two surfaces that have pillars with smaller radius grow bigger droplets, but reached the steady state situation later.

The average heat flux $q$ can be calculated using equation (5) by considering the equal radius instead of $r$. This parameter is shown in figure 18 for each substrate. According to this figure, $q$ decreases by increasing the size of droplets during the process time. Also, by comparing with figure 15 it reveals that the surface with configuration 3, that contains smaller droplets with respect to the other surfaces, presents higher value for $q$. While configuration 1 and 2 that grew bigger droplets show smaller $q$.

Figure 19 shows the percentage of surface area occupied by the droplets on each substrate. According to this figure, the highest percentage is related to the configurations 1 and 6, while the lowest one is related to configuration 2 and the three other substrates represent almost the same value. This figure can be explained by the effect of the texturing pattern that can be interpreted by "how much a pattern makes the substrate different with respect to a flat substrate". In this regard one can use the ratios $\frac{D_p}{r_p} = \frac{\text{distance between the pillars}}{\text{pillars radius}}$ and $\frac{D_p}{H_p} = \frac{\text{distance between the pillars}}{\text{pillars height}}$. These values are presented in table 3. It is clear that when $\frac{D_p}{r_p}$ is smaller means that the pillars

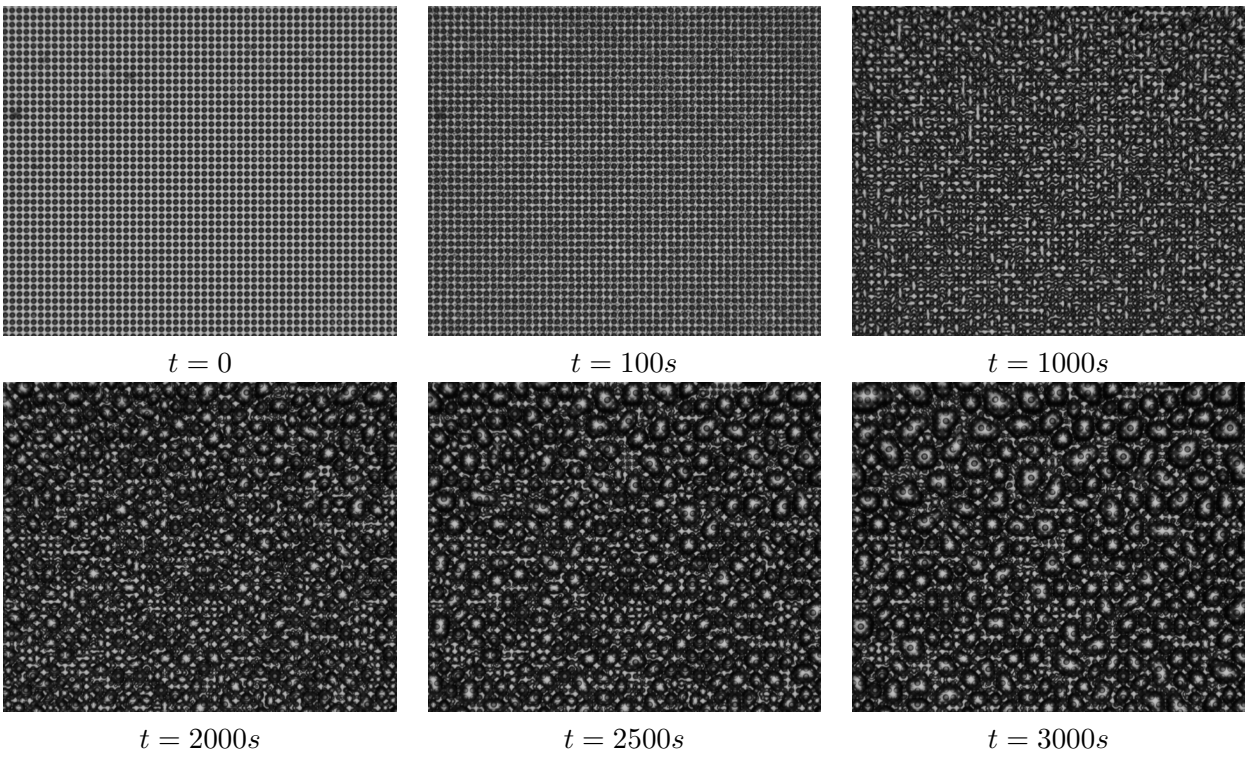


Figure 13: An example of droplets growth procedure on surface configuration 5. The first image shows the pillars just before droplets nucleation. The size of each image is $3.3mm \times 2.7mm$.

Table 3: Each substrate dimensions characteristics.

| configuration of surface | $r_p(\mu m)$ | $D_p$ $(\mu m)$ | $H_p$ $(\mu m)$ | $\frac{D_p}{r_p}$ | $\frac{D_p}{H_p}$ |
|---|---|---|---|---|---|
| configuration 1 | 12.5 | 50 | 3 | 4.0 | 16.7 |
| configuration 2 | 12.5 | 125 | 3 | 6.0 | 41.7 |
| configuration 3 | 25 | 60 | 10 | 2.4 | 6.0 |
| configuration 4 | 25 | 65 | 10 | 2.6 | 6.5 |
| configuration 5 | 25 | 100 | 10 | 4.0 | 10.0 |
| configuration 6 | 25 | 150 | 10 | 6.0 | 15.0 |

cover more area on the substrate. On the other hand, if we consider a canal between the pillars with the length of $D_p$ and the height equal to the height of a pillar, for smaller $\frac{D_p}{H_p}$ the canal prevents the droplets to grow freely and cover more area. This is what happens in the case of configuration 3, 4, and 5 with respect to configurations 1 and 6. On the other hand, when this ratio is two large, it means that the substrate is closer to a flat surface and the texturing pattern does not have any specific effect. This is why configuration 2 represents less percentage of occupied area.

The mean and standard deviation of errors of the proposed model for different configurations of pillars are presented in table 4. In this table mean relative error is calculated as:

$$e = 100 \times \frac{F_{experimental} - F_{model}}{F_{experimental}}, \tag{23}$$

where $F_{experimental}$ is the amount of value calculated based on gray scale images of real droplets and $F_{model}$ is the amount predicted by the simulation model. According to this table, the mean relative error for density of droplets on all of the substrates is $10.00 \pm 0.68\%$, while the model is more accurate for predicting droplets radius with mean relative error of $2.28 \pm 0.42\%$. The error in this model can come from different sources. Firstly, the assumption of the ellipsoidal

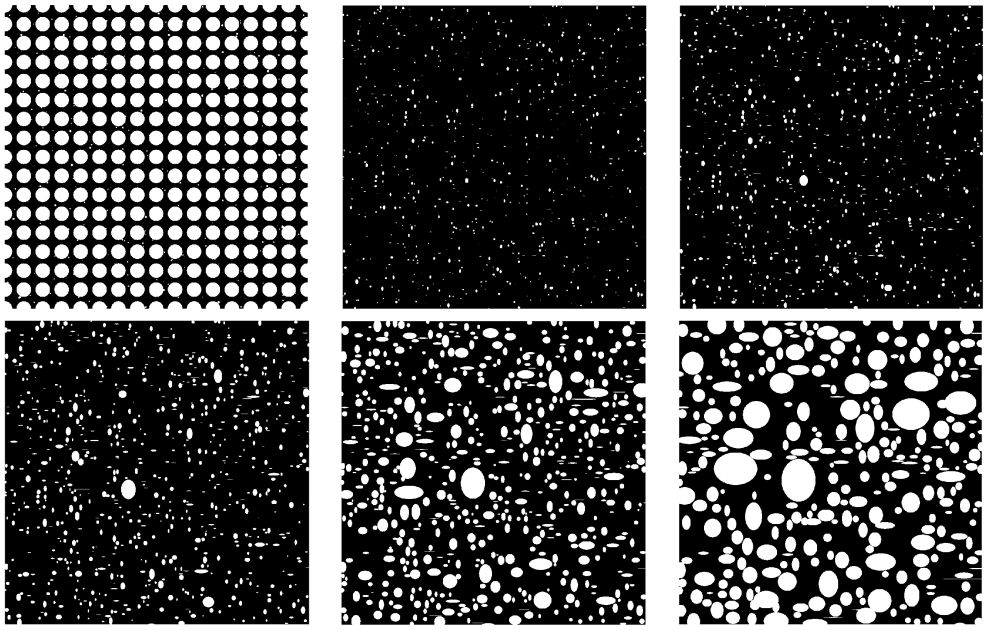

Figure 14: An example of simulated droplets growth procedure on surface configuration 5. The first image shows the pillars just before droplets nucleation. To have a better view of the droplets, the pillars are eliminated from the rest of the images. These images are generated by the simulation algorithm.

droplets is not very accurate although it is more precise than the spherical droplets. For example, according to table 4 the highest error for nucleation density is reported for surface configuration 1, and taking a look at figure 15 reveals that the droplets on this surface have more irregular shapes than the other surfaces. Secondly, the assumption of analogy between ellipsoidal droplets and spherical droplets in calculating the rate of growth due to coalescence, can be another source of error of the model. Thirdly, the difference between $r_p$, $H_p$, and $D_p$ between simulated and real pillars can affect the results also. But, the highest inaccuracy comes from the method of image processing. As was mentioned before, the data related to the size and density of real droplets are extracted from the gray scale images. On the gray scale images taken from the real droplets, the droplets have the same appearance as the pillars, especially when they are in the same size ranges. Both of them are circles with bright centers and dark borders. Moreover in the later stages the droplets are connected and it is difficult to count their exact number. The image processing method that is explained in our earlier work [33] is able to recognize these droplets from the pillars and also is able to separate connected droplets, but we assume that the relatively high error for density of droplets comes mostly from this problem. This can be claimed by comparing the data from table 4 and radius of bigger droplets from figure 16. Surfaces with configuration 1, 4 and 5 that represent higher percentage of error for droplets density, contain droplets that are twice the size of the pillars, while for surface with configuration 2 that the mean error for droplets density is just 3% the droplets are about eight times greater than the pillars and are easily separable from pillars in image processing algorithm. However, it should not be neglected that all these sources of errors lead to an average of error of about 10% for droplets density and 2% for droplets size, so it can be claimed that the ellipsoidal model has a good approximation of the process of dropwise condensation on textured surfaces.

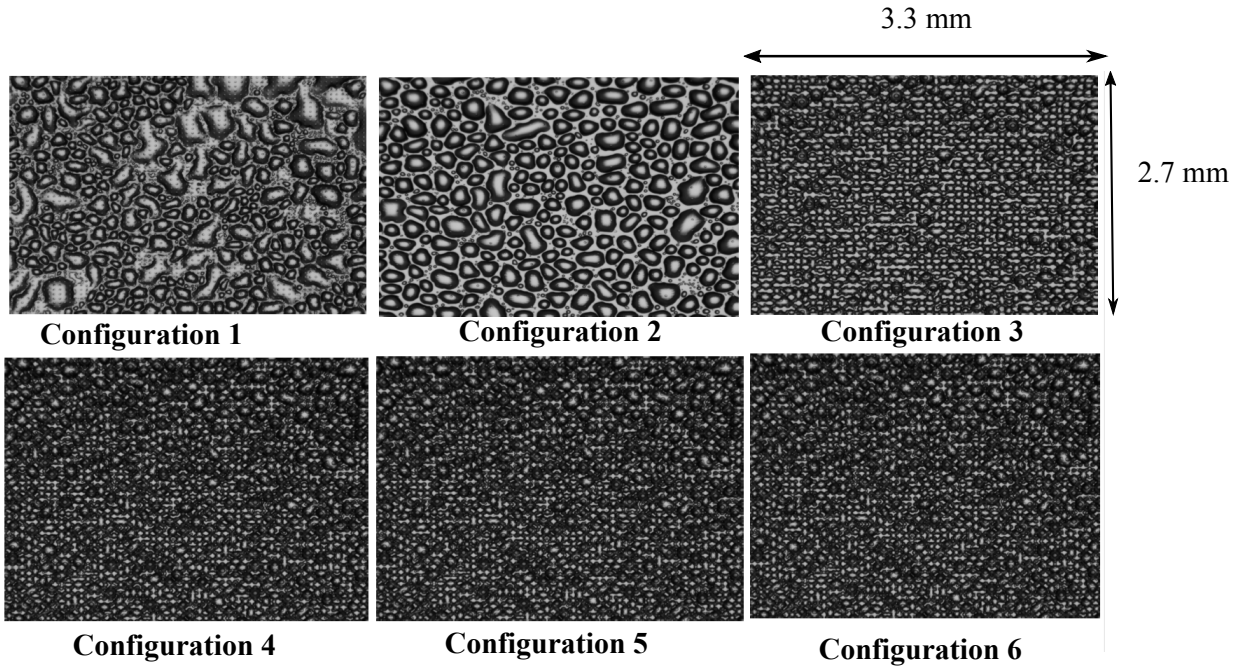


Figure 15: Illustration of 6 pillared surfaces after $1800s$. The size of the substrate at each image is $3.3mm \times 2.7mm$.

Table 4: The mean and standard deviation of errors of the model for different configurations of pillars.

| configuration of pillars | Mean error of density (%) | Mean error of radius (%) |
|---|---|---|
| configuration 1 | 21.28 | -0.62 |
| configuration 2 | 3.55 | 9.26 |
| configuration 3 | 3.01 | -2.01 |
| configuration 4 | 13.14 | 0.18 |
| configuration 5 | 11.33 | 1.80 |
| configuration 6 | 7.7 | 5.04 |
| Mean | $10.00 \pm 0.68$ | $2.28 \pm 0.42$ |

# 7 Conclusion

A numerical model for nucleation and growth of ellipsoidal droplets on three dimensions on pillared substrates has been developed. According to this model ellipsoidal droplets nucleate all around the substrate with three radius $a$, $b$, and $c$ along the axis $X$, $Y$, and $Z$ respectively. Then, these droplets start to grow due to adsorption and coalescence on three dimensions and they can even cover several pillars at final stages. The proposed model is applied to six different pillared surfaces and its mean error is calculated on all the surfaces of about 10% for droplets density and 2% for droplets size. The main source of error is recognized as the similarity between the droplets appearance and pillars on images taken from real droplets, which makes it difficult to identify the exact number of droplets. But, it can be claimed that the proposed model has a good understanding of droplets' growth on pillared substrates.

# 8 Acknowledgments

The authors would like to thank Nicolas Pionnier for the experimental results obtained during his PHD funded by PSA Peugeot-Citroen in the context of OpenLab VAT@Lyon between Peugeot-

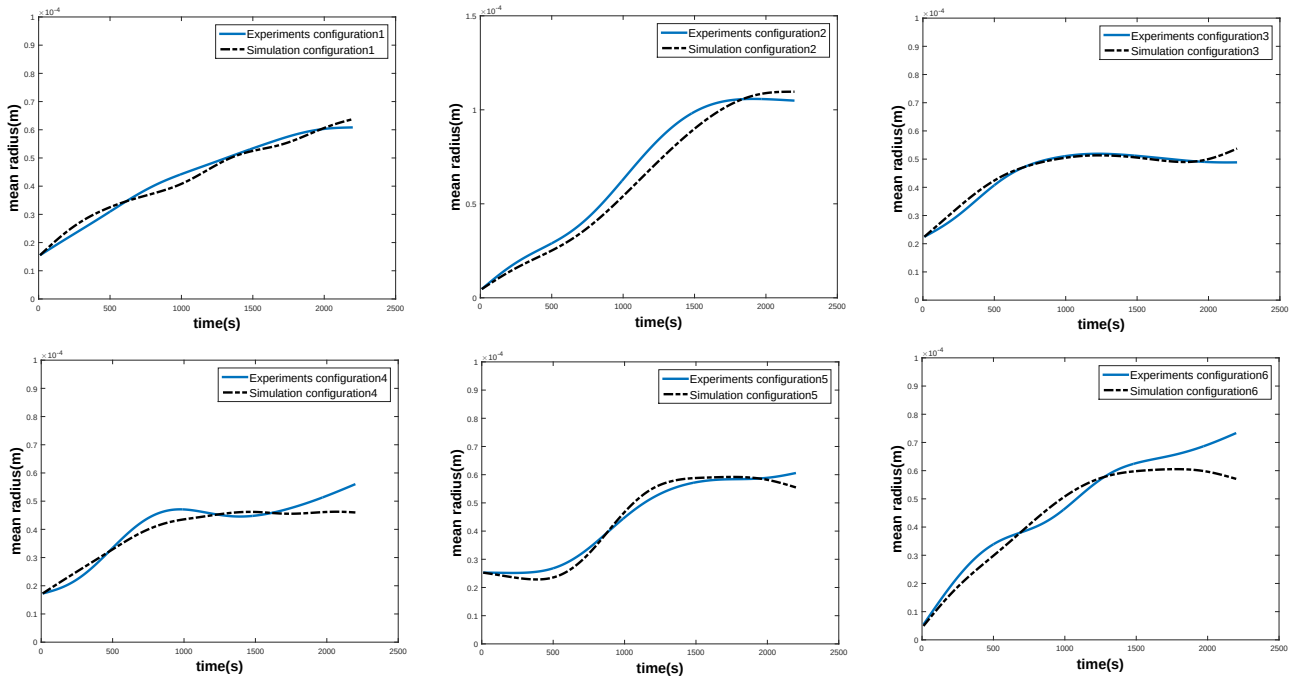


Figure 16: Comparison between growth rate of experimental and simulation droplets on 6 different pillared surfaces. The conditions of experimental procedure are: relative humidity of about 40%, air temperature of 303 K, and substrate temperature of 281 K.

Citroen and LTDS laboratory. This work was funded by LABEX MANUTECH-SISE (ANR-10-LABX-0075, within the program "Investissements d'Avenir" (ANR-11-IDEX-0007) operated by the French National Research Agency (ANR).

## References

[1] D Beysens. The formation of dew. *Atmospheric research*, 39(1-3):215–237, 1995.

[2] Yongpan Cheng, Jinliang Xu, and Yi Sui. Numerical investigation of coalescence-induced droplet jumping on superhydrophobic surfaces for efficient dropwise condensation heat transfer. *International Journal of Heat and Mass Transfer*, 95:506–516, 2016.

[3] Jonathan B Boreyko, Yuejun Zhao, and Chuan-Hua Chen. Planar jumping-drop thermal diodes. *Applied Physics Letters*, 99(23):234105, 2011.

[4] Nenad Miljkovic, Ryan Enright, and Evelyn N Wang. Modeling and optimization of superhydrophobic condensation. *Journal of Heat Transfer*, 135(11):111004, 2013.

[5] E Schmidt, W Schurig, and W Sellschopp. Versuche über die kondensation von wasserdampf in film-und tropfenform. *Technische Mechanik und Thermodynamik*, 1(2):53–63, 1930.

[6] Ramchandra D Narhe, Wenceslao González-Viñas, and Daniel A Beysens. Water condensation on zinc surfaces treated by chemical bath deposition. *Applied Surface Science*, 256(16):4930–4933, 2010.

[7] Daniel Beysens. Dew nucleation and growth. *Comptes Rendus Physique*, 7(9-10):1082–1100, 2006.

[8] D Beysens, V Pruvost, and B Pruvost. Dew observed on cars as a proxy for quantitative measurements. *Journal of Arid Environments*, 135:90–95, 2016.

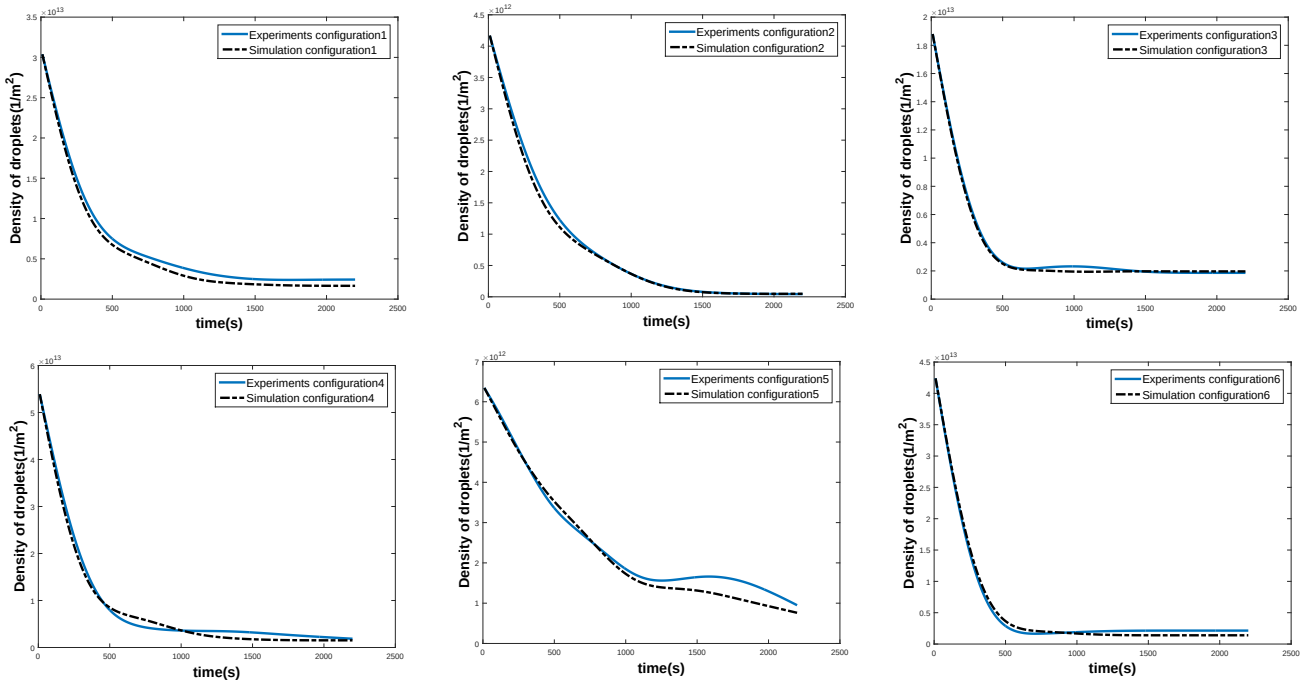


Figure 17: Comparing the changes in droplets density between experimental and simulation droplets on 6 different pillared surfaces. The conditions of experimental procedure are: relative humidity of about 40%, air temperature of 303 K, and substrate temperature of 281 K.


[9] Maofei Mei, Feng Hu, Chong Han, and Yanhai Cheng. Time-averaged droplet size distribution in steady-state dropwise condensation. *International Journal of Heat and Mass Transfer*, 88:338–345, 2015.

[10] Leon R Glicksman and Andrew W Hunt. Numerical simulation of dropwise condensation. *International Journal of Heat and Mass Transfer*, 15(11):2251–2269, 1972.

[11] S Vemuri and KJ Kim. An experimental and theoretical study on the concept of dropwise condensation. *International journal of heat and mass transfer*, 49(3):649–657, 2006.

[12] Tianyi Song, Zhong Lan, Xuehu Ma, and Tao Bai. Molecular clustering physical model of steam condensation and the experimental study on the initial droplet size distribution. *International Journal of Thermal Sciences*, 48(12):2228–2236, 2009.

[13] Xiuliang Liu and Ping Cheng. Dropwise condensation theory revisited part ii. droplet nucleation density and condensation heat flux. *International Journal of Heat and Mass Transfer*, 83:842–849, 2015.

[14] John Francis Welch. *Microscopic study of dropwise condensation*. PhD thesis, University of Illinois at Urbana-Champaign, 1961.

[15] Hamid Reza Talesh Bahrami and Hamid Saffari. Theoretical study of stable dropwise condensation on an inclined micro/nano-structured tube. *International Journal of Refrigeration*, 75:141–154, 2017.

[16] Robert N Wenzel. Resistance of solid surfaces to wetting by water. *Industrial & Engineering Chemistry*, 28(8):988–994, 1936.

[17] ABD Cassie and S Baxter. Wettability of porous surfaces. *Transactions of the Faraday society*, 40:546–551, 1944.

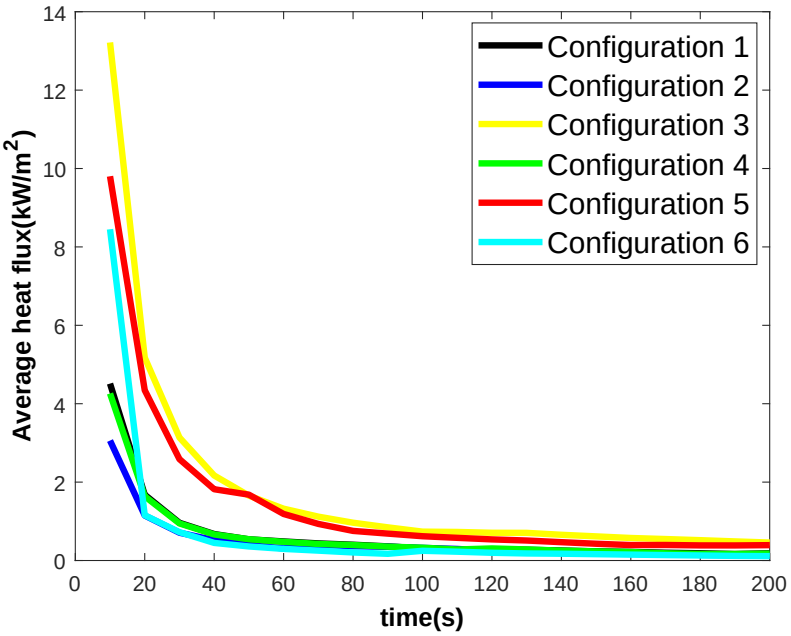


Figure 18: Average heat flux for each substrate.


[18] Takahiro Koishi, Kenji Yasuoka, Shigenori Fujikawa, Toshikazu Ebisuzaki, and Xiao Cheng Zeng. Coexistence and transition between cassie and wenzel state on pillared hydrophobic surface. *Proceedings of the National Academy of Sciences*, 106(21):8435–8440, 2009.

[19] Chuan-Hua Chen, Qingjun Cai, Chialun Tsai, Chung-Lung Chen, Guangyong Xiong, Ying Yu, and Zhifeng Ren. Dropwise condensation on superhydrophobic surfaces with two-tier roughness. *Applied Physics Letters*, 90(17):173108, 2007.

[20] M Qian and J Ma. The characteristics of heterogeneous nucleation on concave surfaces and implications for directed nucleation or surface activity by surface nanopatterning. *Journal of Crystal Growth*, 355(1):73–77, 2012.

[21] M Gazicki, WJ James, and HK Yasuda. Colloids and surfaces a: Physicochemical and engineering aspects. *Journal of Polymer Science: Letters Polymer Edition*, 23:639–645, 1985.

[22] Eli Ruckenstein and Gersh O Berim. Kinetics of heterogeneous nucleation on a rough surface: Nucleation of a liquid phase in nanocavities. *Journal of colloid and interface science*, 351(1):277–282, 2010.

[23] Gersh O Berim and Eli Ruckenstein. Kinetic theory of heterogeneous nucleation; effect of nonuniform density in the nuclei. *Journal of colloid and interface science*, 355(1):259–264, 2011.

[24] Saeed Zarei, Hamid Reza Talesh Bahrami, and Hamid Saffari. Effects of geometry and dimension of micro/nano-structures on the heat transfer in dropwise condensation: A theoretical study. *Applied Thermal Engineering*, 137:440–450, 2018.

[25] S Boroomandi Barati, N Pionnier, J-C Pinoli, S Valette, and Y Gavet. Investigation spatial distribution of droplets and the percentage of surface coverage during dropwise condensation. *International Journal of Thermal Sciences*, 124:356–365, 2018.

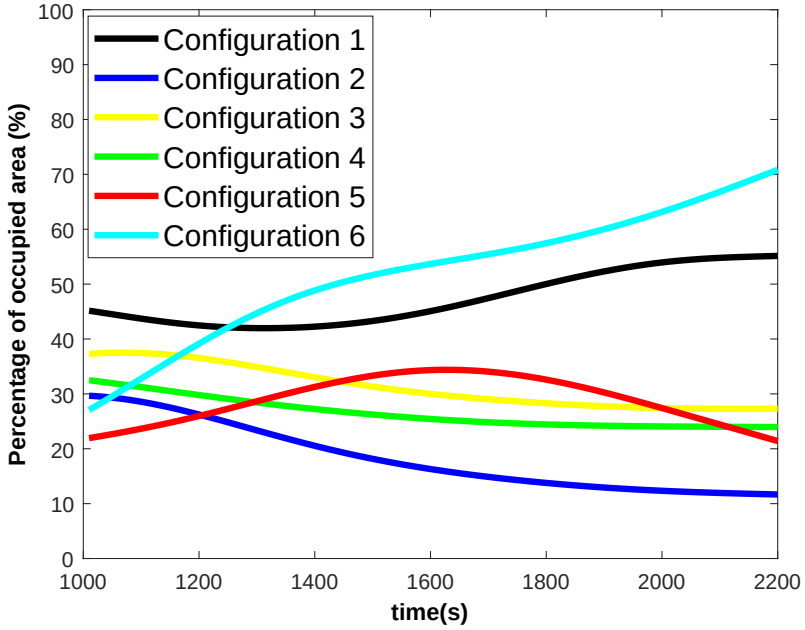


Figure 19: percentage of surface coverage at steady state for each substrate.


[26] Solmaz Boroomandi Barati, Jean-Charles Pinoli, Stephane Valette, and Yann Gavet. Differential and average approaches to rose and mei dropwise condensation models. In *INASE-MMSSE 2017-The 2017 International Conference on Mathematical Methods, Mathematical Models and Simulation in Science and Engineering*, volume 11, pages 40–à. North Atlantic University Union, 2017.

[27] D Niu, L Guo, HW Hu, and GH Tang. Dropwise condensation heat transfer model considering the liquid-solid interfacial thermal resistance. *International Journal of Heat and Mass Transfer*, 112:333–342, 2017.

[28] Nenad Miljkovic, Ryan Enright, and Evelyn N Wang. Growth dynamics during dropwise condensation on nanostructured superhydrophobic surfaces. In *ASME 2012 Third International Conference on Micro/Nanoscale Heat and Mass Transfer*, pages 427–436. American Society of Mechanical Engineers, 2012.

[29] Nenad Miljkovic and Evelyn N Wang. Condensation heat transfer on superhydrophobic surfaces. *MRS bulletin*, 38(5):397–406, 2013.

[30] Michael Nosonovsky. Model for solid-liquid and solid-solid friction of rough surfaces with adhesion hysteresis. *The Journal of chemical physics*, 126(22):224701, 2007.

[31] Mousa Abu-Orabi. Modeling of heat transfer in dropwise condensation. *International journal of heat and mass transfer*, 41(1):81–87, 1998.

[32] Contraires S Berger R Guibert M Benayoun S Valette S Pionnier N, Boroomandi Barati S. Design of an environment controlled dew tracking setup to emphasize the role of the relative humidity on breath figures dynamics. *EPJ journal of thecniques and instrumentation*, 5(2), 2018.

[33] Helene Martin, Solmaz Boroomandi Barati, Jean-Charles Pinoli, Stephane Valette, and Yann Gavet. Segmentation of gray scale images of dropwise condensation on textured surfaces. *World Academy of Science, Engineering and Technology, International Journal of Computer and Information Engineering*, 5(1):115–126, 2018.

[34] Ichiro Tanasawa. Advances in condensation heat transfer. *Advances in heat transfer*, 21:55–139, 1991.